

Determination of the size of the dust torus in H0507+164 through optical and infrared monitoring

Amit Kumar Mandal^{1,2*}, Suwendu Rakshit^{1,3†}, Kshama S. Kurian¹, C. S. Stalin^{1‡}, Blesson Mathew², Sebastian Hoenig⁴, Poshak Gandhi⁴, Ram Sagar¹ and M. B. Pandge^{5§}

¹Indian Institute of Astrophysics, Block II, Koramangala, Bangalore 560 034, India

²Department of Physics, Christ University, Hosur Road, Bangalore 560 029, India

³Astronomy Program, Department of Physics and Astronomy, Seoul National University, Seoul 151-742, Republic of Korea

⁴Department of Physics & Astronomy, University of Southampton, Southampton SO17 1BJ, UK

⁵Dayanand Science College, Barshi Road, Latur, Maharashtra 413512, India

Accepted 2018 January 19. Received 2018 January 11; in original form 2017 September 5

ABSTRACT

The time delay between flux variations in different wavelength bands can be used to probe the inner regions of active galactic nuclei (AGN). Here, we present the first measurements of the time delay between optical and near-infrared (NIR) flux variations in H0507+164, a nearby Seyfert 1.5 galaxy at $z = 0.018$. The observations in the optical V -band and NIR J , H and K_s bands carried over 35 epochs during the period October 2016 to April 2017 were used to estimate the inner radius of the dusty torus. From a careful reduction and analysis of the data using cross-correlation techniques, we found delayed responses of the J , H and K_s light curves to the V -band light curve. In the rest frame of the source, the lags between optical and NIR bands are found to be $27.1^{+13.5}_{-12.0}$ days (V vs. J), $30.4^{+13.9}_{-12.0}$ days (V vs. H) and $34.6^{+12.1}_{-9.6}$ days (V vs. K_s). The lags between the optical and different NIR bands are thus consistent with each other. The measured lags indicate that the inner edge of dust torus is located at a distance of 0.029 pc from the central UV/optical AGN continuum. This is larger than the radius of the broad line region of this object determined from spectroscopic monitoring observations thereby supporting the unification model of AGN. The location of H0507+164 in the $\tau - M_V$ plane indicates that our results are in excellent agreement with the now known lag-luminosity scaling relationship for dust in AGN.

Key words: galaxies: active – galaxies: Seyfert – (galaxies:) quasars: individual (H0507+164)

1 INTRODUCTION

Active Galactic Nuclei (AGN) are among the most luminous objects in the Universe that produce very high luminosity in a very concentrated volume, powered by the accretion of matter onto super-massive black hole (SMBH) located at the centers of galaxies. According to the unified model of AGN, a dusty torus that surrounds the central SMBH, the accretion disk and the broad line region (BLR) play a key role in the identification of Seyfert galaxies, a category of AGN, into

Seyfert 1 and Seyfert 2 galaxies (Antonucci 1993). Evidence for their presence is seen in the broad band spectral energy distribution (SED) of AGN, such as the presence of the big blue bump in the optical-UV wavelength region, which is a signature of the accretion disk (Czerny & Elvis 1987; Malkan & Sargent 1982; Shields 1978) and a bump in the IR region (Sanders et al. 1989; Barvainis 1987; Kobayashi et al. 1993) which is a signature of the presence of the dusty torus.

The torus, which obscures the central engine, is the dominant source of IR radiation in most of the AGN. It is not easy to spatially resolve the components of the AGN such as the BLR and torus by any current imaging techniques. The IR radiation of AGN coming from the torus that extends in size from sub-pc to pc size scales (Kishimoto et al. 2011a)

* E-mail: amitkumar@iiap.res.in

† E-mail: suwenduat@gmail.com

‡ E-mail: stalin@iiap.res.in

§ DST INSPIRE Faculty

could in principle be resolvable using IR interferometric observations. However, such interferometric observations as of today are in a minority (Kishimoto et al. 2011b; Burtscher et al. 2013) and limited by the current diameters of optical/IR telescopes. Alternatively, the extent and nature of the torus can be studied via the technique of reverberation mapping (Blandford & McKee 1982). This technique relies on the flux variability of AGN, which has been known since their discovery. The continuum emission from AGN is believed to arise from the accretion disk and it is expected to vary over a range of time scales from hours to days. The variations in the continuum flux are observed at a later time in the fluxes of their broad emission lines. Similarly, there is also delayed response of the IR continuum emission (from the torus) to the changes in the optical continuum from the central AGN, which indicates that the NIR continuum and UV/optical continuum emission are causally connected. This delay between the optical and IR variation when measured can give the radius of the inner most hot dust torus $r_{\text{dust}} = \tau \times c$, where c is the speed of light and τ is the time delay between optical and IR variations. This method of measuring the delayed response of the IR emission relative to the optical emission and consequently determine the size of the torus is referred to as dust reverberation mapping (DRM).

Studies of DRM in few Seyfert galaxies (Minezaki et al. 2004; Suganuma et al. 2006; Koshida et al. 2014) have led to the establishment of a correlation between the inner radius of the dust torus and the UV luminosity as $r_{\text{dust}} \propto L^{0.5}$ (Kishimoto et al. 2007). Also, Kishimoto et al. (2007) established a relation between the sublimation radius (R_{sub}) which is defined as the radius at which dust particle sublimates and the dust grain size (a) as

$$R_{\text{sub}} = 1.3 \left(\frac{L_{UV}}{10^{46} \text{ergs}^{-1}} \right)^{0.5} \left(\frac{T_{\text{sub}}}{1500 \text{K}} \right)^{-2.8} \left(\frac{a}{0.05 \mu\text{m}} \right)^{-0.5} \text{ pc} \quad (1)$$

Considering sublimation temperature (T_{sub}) to be the dust temperature $T_{\text{dust}} = 1700 \text{ K}$ which was evaluated from the NIR colors of the variable flux component for Seyfert 1 galaxies (Tomita et al. 2006; Koshida et al. 2014) and grain size $a = 0.1 \mu\text{m}$, the sublimation radius from equation 1 can be written as $\log R_{\text{sub}}/\text{pc} = -0.80 + 0.5 \log(L_V/10^{44} \text{ erg s}^{-1})$, where $L_{UV} = 6 L_V$ (Kishimoto et al. 2007). This is in excellent agreement with the relation of $\log r_{\text{dust}}/\text{pc} = -0.88 + 0.5 \log(L_V/10^{44} \text{ erg s}^{-1})$ obtained by a linear regression fit to the reverberation mapping data of a few Seyfert galaxies by Koshida et al. (2014). Thus, DRM observations using the K -band in the infrared region can define the inner radius of the dust torus for an AGN.

The emission line lag (e.g., Watson et al. 2011; Haas et al. 2011; Czerny et al. 2013) and dust reverberation lag (e.g., Oknyanskij et al. 1999; Oknyanskij & Horne 2001; Hönig 2014; Yoshii et al. 2014; Hönig et al. 2017) have been proposed to serve as standard candles. However, the later shows a stronger correlation between lag and luminosity than former and needs only photometric monitoring making it preferable for standard candle although the emission line lags can be measured up to $z \sim 4$ (see Watson et al. 2011). Unfortunately, only handful number of objects has dust lag measurement (Suganuma et al. 2006; Pozo Nuñez et al. 2014; Koshida et al. 2014), which motivated Hönig et al. (2017) to carry out a large dust reverberation map-

ping (DRM) program, “VEILS” (VISTA Extragalactic Infrared Legacy Survey) to use dust lag as standard candle for cosmology and constrain cosmological parameters. The “VEILS” survey will target about 1350 Seyfert 1 galaxies in the redshift range $0.1 < z < 1.2$, however, missing the objects in the local universe which are crucial in determining the normalization parameter of the AGN distance moduli (see Hönig et al. 2017). Thus, dust reverberation mapping of local AGN will not only allow to estimate the extent of the torus, dust morphology and verify orientation dependent unification model but also help to estimate the normalization constant of the Hubble function.

To complement the VEILS program, in the nearby Universe, we are carrying out monitoring observations of a carefully selected sample of AGN with redshift less than 0.1 as part of our long term project called REMAP (REverberation Mapping of AGN Program). Observations towards this project has been carried out using the 2 m Himalayan Chandra Telescope at Hanle, India. Such a systematic study in conjunction with VEILS will serve as an excellent database to probe the complex interplay between optical continuum and dust emission in AGN. Here, we present the results of DRM monitoring of one local ($z = 0.018$) Seyfert 1.5 galaxy H0507+164. The structure of this paper is as follows. In section 2 we briefly describe the observation and data reduction processes. The analysis is presented in section 3. The results are discussed in section 4 followed by the summary in section 5. For the cosmological parameters we assumed $H_0 = 73 \text{ km s}^{-1} \text{ Mpc}^{-1}$, $\Omega_m = 0.27$ and $\Omega_\lambda = 0.73$ (Koshida et al. 2014).

2 OBSERVATION AND DATA REDUCTION

2.1 The Sample

The sample of sources for our DRM project were drawn from Bentz & Katz (2015) that have BLR lag from spectroscopic reverberation observations. From this list, we have selected only those sources that are accessible for observations using the 2m Himalayan Chandra Telescope (HCT) located at Hanle and operated by the Indian Institute of Astrophysics¹. In this paper, we present the result of the first source monitored for DRM using the HCT, namely H0507+164, a local Seyfert 1.5 galaxy at $z = 0.018$ with RA = 05:10:45.5 and DEC = +16:29:56. It is bright with an optical g band magnitude of 10 mag from the SIMBAD database². It has a black hole mass of $9.62^{+0.33}_{-3.73} \times 10^6 M_\odot$ deduced from spectroscopic reverberation observations (Stalin et al. 2011). It is detected in the NRAO/VLA Sky Survey (NVSS³) with a flux density of $6 \pm 0.5 \text{ mJy}$ at 1.4 GHz. However, it is radio quiet with a radio loudness parameter, R (ratio of flux density in the radio-band at 1.4 GHz to the optical V -band flux density) of 2.26 ± 0.26 .

2.2 Observations

The observations were carried out for a total of 35 epochs during the period October 2016 to April 2017 using HCT

¹ <http://www.iiap.res.in/centres/iao>

² <http://simbad.u-strasbg.fr/simbad/>

³ <http://www.cv.nrao.edu/nvss/nvsslist.shtml>

The telescope is a Ritchey-Chretien system with an $f/9$ beam. The optical observations were carried out using the Himalayan Faint Object Spectrograph and Camera (HFOSC) mounted at the Cassegrain focus and equipped with a $2K \times 4K$ SiTe CCD system. This CCD has a read-out noise and gain of 4.8 electrons/ADU and 1.22 electrons respectively. The observations were carried out in binned mode using only the central $2K \times 2K$ region. Each pixel of the CCD in this mode corresponds to 0.3×0.3 arcsec², and for the imaging observations reported here has a field of view of 10×10 arcmin². The typical exposure time in V -band is about 50 seconds. The IR observations in J , H and K_s bands were done subsequently to the V -band observations at each epoch were carried out using the TIFR Near Infrared Spectrometer (TIRSPEC) mounted on one of the side ports of HCT (Ninan et al. 2014). The detector used in TIRSPEC is a 1024×1024 HgCdTe array with a pixel size of $18 \mu\text{m}$ covering a field of view of 5×5 arcmin². It has a readout noise and gain of 25 electrons and 6 electrons/ADU respectively. The IR observations were performed in dithered mode consisted of five exposures each of 20 sec at three dither positions for each of three IR filters namely J , H and K_s . Apart from the science frames, sky regions were also observed in the same dithering pattern as the object to generate master sky frame.

2.3 Data reduction

The optical data reduction was done using IRAF (Image Reduction and Analysis Facility⁴) and MIDAS (Munich Data Analysis System⁵). For image reduction, we followed the standard procedure, such as bias & dark subtraction and flat-fielding. After removing the cosmic rays, the optical frames were aligned and then combined using `imalign` and `imcombine` tasks in IRAF for each day. Point spread function (PSF) photometry was carried out on the combined images using the `daophot` and `allstar` packages in MIDAS to find the instrumental magnitudes of the object and the comparison stars present in the CCD frames. The observed V -band image is shown in Figure 1.

Reduction of the NIR images was performed using TIRSPEC NIR Data Reduction Pipeline (Ninan et al. 2014) for each band. The pipeline subtracts the dark obtained for the same exposure time as the science exposures and then uses twilight flats for flat fielding and produce final combined images. PSF photometry on the combined images was carried out by using MIDAS to get the instrumental magnitudes.

The object appears as a point source in our optical and IR data, thereby, making it difficult to model the host galaxy from the observed data and remove its contribution to the measured brightness. Therefore, subtraction of the host galaxy contribution to the measured brightness of the source was not carried out. Also, we have not corrected the observed flux values for galactic extinction. These effects will



Figure 1. Observed V -band image of H0507+164. The integration time is 50 seconds and each side is 10 arcmin. The target source is shown with a circle.

be small and a constant fraction of the measured flux values, thus having negligible effects on the cross-correlation analysis.

2.4 Subtraction of the accretion disk component from the NIR bands

The observed NIR fluxes are dominated by emission from the torus due to re-processing of the central UV/optical emission by the hot dust. However, it is contaminated by variable flux from the accretion disk component (Tomita et al. 2006; Kishimoto et al. 2008; Lira et al. 2011). This would make the time lag calculated by cross correlation analysis between the optical and IR light curves shorter than the actual lag of the dust-torus emission (Koshida et al. 2014). Thus, to get the true time lag, between optical and NIR flux variations, the contribution of accretion disk to the measured NIR fluxes needs to be removed. We estimated the contribution of the accretion disk in the J , H , K_s -bands in each of the epochs of observations by considering a power-law spectrum of the accretion disk following Koshida et al. (2014) and given by

$$f_{\text{NIR,disk}}(t) = f_V(t) \left(\frac{\nu_{\text{NIR}}}{\nu_V} \right)^{\alpha_\nu} \quad (2)$$

where, $f_V(t)$ is the V -band flux at time ‘ t ’, ν_V and ν_{NIR} are effective frequencies of V -band and NIR bands respectively and α_ν is the power-law index. At any given epoch, the observations in the optical and each of the NIR bands differ by less than 300 seconds, and therefore, for the purpose of removing the contribution of accretion disk to each of the NIR bands, they were considered as simultaneous observations. To calculate $f_{\text{NIR,disk}}(t)$, we assumed power-law index α_ν to be equal to $1/3$ following Koshida et al. (2014). AGN do show spectral variability with a bluer-when-brighter behavior (Meusinger et al. 2011) which demands adoption of a time dependent α_ν to correct for the contribution of accretion disk emission to NIR. Our single optical V -band

⁴ IRAF is operated by the Association of Universities for Research in Astronomy, Inc., under cooperative agreement with the National Science Foundation.

⁵ MIDAS is the trade-mark of the European Southern Observatory

Table 1. Log of observations and results of photometry. Here JD is in days, the fluxes in different bands and their associated errors are in units of 10^{-26} erg s $^{-1}$ cm $^{-2}$ Hz $^{-1}$.

JD _V	F _V	σ _V	JD _J	F _J	σ _J	JD _H	F _H	σ _H	JD _{K_s}	F _{K_s}	σ _{K_s}
2457687.4272	3.295	0.260	2457687.4429	4.994	0.302	2457687.4374	7.628	0.517	2457687.4316	12.582	0.490
2457693.2663	3.129	0.247	2457693.2765	5.519	0.312	2457693.2819	8.521	0.457	2457693.2875	12.835	0.399
2457697.2763	3.115	0.246	2457697.2802	6.027	0.313	2457697.2858	9.339	0.432	2457697.2950	13.585	0.387
2457699.4455	2.784	0.221	2457699.4277	5.161	0.346	2457699.4219	7.520	0.399	2457699.4164	12.783	1.174
2457700.2714	2.999	0.238	2457700.2536	6.287	0.521	2457700.2473	9.262	0.429	2457700.2416	13.473	0.386
2457704.2750	3.019	0.238	2457704.2595	6.008	0.305	2457704.2541	9.459	0.428	2457704.2486	13.589	0.403
2457710.2058	3.331	0.262	2457710.2274	6.596	0.317	2457710.2219	9.989	0.455	2457710.2165	14.439	0.422
2457711.3872	3.064	0.241	2457711.3110	6.768	0.357	2457711.3051	9.962	0.447	2457711.2986	13.995	0.621
2457712.3179	3.041	0.240	2457712.3339	6.710	0.453	2457712.3279	8.612	0.415	2457712.3219	12.946	0.416
2457717.4375	3.129	0.247	2457717.4540	5.734	0.324	2457717.4488	9.297	0.441	2457717.4435	14.027	0.536
2457719.2792	3.365	0.265	2457719.3544	7.811	0.384	2457719.3489	10.171	0.543	2457719.3433	15.470	0.668
2457721.2253	2.668	0.212	2457721.2420	5.685	0.289	2457721.2364	9.295	0.526	2457721.2308	13.682	0.440
2457727.1733	2.690	0.213	2457727.1922	5.747	0.394	2457727.1868	9.270	0.518	2457727.1812	14.099	0.472
2457728.4147	2.596	0.206	2457728.3990	6.519	0.523	2457728.3928	8.346	0.411	2457728.3874	12.835	0.422
2457732.2453	2.451	0.194	2457732.2619	5.852	0.318	2457732.2559	9.073	0.401	2457732.2499	14.018	0.423
2457739.4652	2.560	0.205	2457739.4483	5.804	0.276	2457739.4421	9.983	0.415	2457739.4363	13.936	0.382
2457745.2972	1.974	0.158	2457745.2543	5.352	0.374	2457745.2485	8.704	0.364	2457745.2420	13.121	0.365
2457750.3023	1.985	0.158	2457750.0752	5.175	0.327	2457750.0811	8.368	0.371	2457750.0890	12.969	0.394
2457752.3102	2.004	0.162	2457752.3535	6.695	0.262	2457752.3476	10.556	0.411	2457752.3415	14.664	0.403
2457768.0595	2.651	0.213	2457768.0408	5.642	0.307	2457768.0331	8.345	0.385	2457768.0276	12.681	0.376
2457773.3053	3.086	0.243	2457773.2892	6.372	0.302	2457773.2830	9.025	0.413	2457773.2769	12.876	0.389
2457784.1059	2.163	0.173	2457784.1302	3.666	0.316	2457784.1220	7.208	0.372	2457784.1136	10.684	0.355
2457788.2195	2.171	0.173	2457788.2422	4.591	0.392	2457788.2362	7.938	0.422	2457788.2302	14.780	0.528
2457794.2058	2.065	0.164	2457794.2221	5.169	0.386	2457794.2160	6.960	0.363	2457794.2104	10.702	0.350
2457801.1541	1.982	0.158	2457801.1683	4.076	0.226	2457801.1626	6.604	0.338	2457801.1568	11.091	0.356
2457807.0827	1.868	0.149	2457807.0662	4.963	0.350	2457807.0598	6.646	0.314	2457807.0538	10.771	0.339
2457808.2595	2.497	0.197	2457808.2429	5.374	0.244	2457808.2372	8.461	0.369	2457808.2315	11.685	0.324
2457812.2031	2.052	0.166	2457812.1793	4.063	0.238	2457812.1733	6.533	0.356	2457812.1673	10.096	0.439
2457817.1344	2.169	0.173	—	—	—	2457817.1214	4.961	0.317	2457817.0465	10.255	0.356
2457829.0926	2.326	0.186	2457829.0757	4.414	0.261	2457829.0698	6.161	0.344	2457829.0639	9.997	0.359
2457832.1700	2.586	0.206	2457832.1545	4.882	0.251	2457832.1483	8.705	0.425	2457832.1470	10.143	0.306
2457838.1930	2.972	0.235	2457838.1716	4.650	0.287	2457838.1656	7.371	0.374	2457838.1601	10.626	0.333
2457847.1147	3.061	0.243	2457847.1010	4.989	0.422	2457847.0918	7.763	0.389	2457847.0861	10.814	0.411
2457851.1541	3.289	0.265	2457851.1399	5.507	0.306	2457851.1344	8.052	0.399	2457851.1289	11.519	0.436
2457858.1201	3.078	0.244	2457858.1044	6.078	0.356	2457858.0989	8.170	0.414	2457858.0933	11.727	0.373

observations hinder determination of α_ν for each epoch of our observations. Use of single α_ν might have some effect on the corrected J -band fluxes, however, it will have negligible effect on the corrected K_s -band flux values.

Prior to the calculation and subsequent subtraction of the accretion disk component from the observed NIR fluxes, the observed instrumental magnitudes were converted to apparent magnitudes via differential photometry of few stars in the field whose apparent magnitudes were taken from the SIMBAD database. The apparent magnitudes were then corrected for Galactic extinction taken from the NASA/IPAC Extragalactic database (NED⁶). These magnitudes were then converted into fluxes and the contribution of accretion disk evaluated using equation 2 were subtracted. The final fluxes thus obtained were used to generate optical and NIR light curves for further analysis. The errors in the final flux values in different filters were obtained through propagation of errors during the various steps of flux determination.

3 ANALYSIS

3.1 Light curves

The light curves of H0507+164 in optical V -band and NIR J , H and K_s bands are shown in Figure 2. As the source is radio-quiet, not much contamination to the observed flux variations is expected from the jet of the source. The variability nature of the source was characterized using the normalized excess variance (Edelson et al. 2002; Vaughan et al. 2003; Rani et al. 2017) defined as

$$F_{\text{var}} = \frac{\sqrt{S^2 - \delta^2}}{\langle f \rangle} \quad (3)$$

Here $\langle f \rangle$, S^2 , δ are the mean flux, variance and mean

⁶ <https://ned.ipac.caltech.edu/>

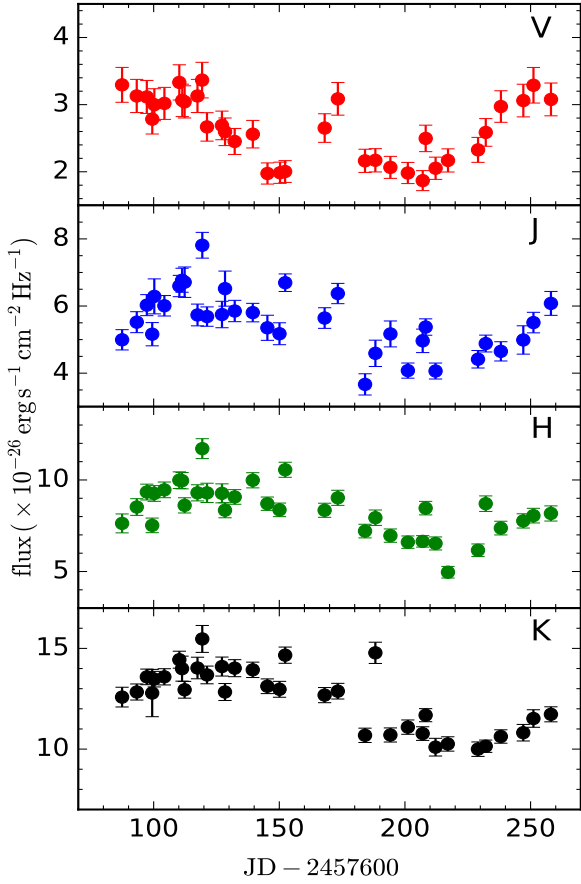


Figure 2. The light curves of H0507+164 in V , J , H , K_s -bands for the period from October 2016 to February 2017. The NIR light curves were corrected for the contamination of emission from the accretion disk.

error respectively for N observations and are given as

$$\langle f \rangle = \frac{1}{N} \sum_{i=1}^N f_i \quad (4)$$

$$S^2 = \frac{1}{N-1} \sum_{i=1}^N (f_i - \langle f \rangle)^2 \quad (5)$$

$$\delta^2 = \frac{1}{N} \sum_{i=1}^N \delta_i^2, \quad (6)$$

$$(7)$$

where f_i and δ_i are the flux and error for the i^{th} measurement respectively. The uncertainties in the F_{var} are evaluated following Edelson et al. (2002) and given as

$$\text{err}(F_{\text{var}}) = \sqrt{\left(\sqrt{\frac{1}{2N} \frac{\delta^2}{\langle f \rangle^2 F_{\text{var}}}} \right)^2 + \left(\sqrt{\frac{\delta^2}{N} \frac{1}{\langle f \rangle}} \right)^2} \quad (8)$$

In addition to calculating F_{var} we also calculated the ratio R_{max} between the maximum and minimum flux in the light curves. The results of variability analysis are given in Table 2. It is noticed that F_{var} in the optical V -band and NIR J and H -bands are similar, while the F_{var} in K_s band is lower than that in the other bands. An anti-correlation between variability amplitude and wavelength has been found

Table 2. Variability statistics in $VJHK_s$ bands in observer's frame. Here, λ_{eff} is the effective wavelength in Angstroms. The average values ($\langle f \rangle$) and the standard deviation σ of the $VJHK_s$ light curves

Filter	λ_{eff}	$\langle f \rangle$	σ	F_{var}	R_{max}
V	5510	2.66	0.48	0.159 ± 0.005	1.801
J	12200	5.56	0.89	0.149 ± 0.003	2.131
H	16300	8.39	1.36	0.154 ± 0.002	2.360
K_s	21900	12.56	1.56	0.119 ± 0.001	1.548

recently based on analysis of NIR variability of a large sample of AGN by Sánchez et al. (2017). Also, compared to the optical bands, amplitude of NIR variation is expected to be smaller (Enya et al. 2002). Though our data do not reveal a clear anti-correlation of variability amplitude with wavelength as found recently (Sánchez et al. 2017), the F_{var} in the NIR bands are lower than of the optical V -band as expected (Enya et al. 2002). Therefore, the low amplitude of variations seen in the K_s band do not point to any inherent bias in the K_s band data.

3.2 Cross-Correlation Analysis

Our observations indicate that the source H0507+164 show flux variations in the optical and NIR bands enabling us to test for the presence/absence of time delay between flux variations in different bands. To calculate the time lag between the variations in the optical V -band emission from the accretion disk and the IR emission from the torus, we employed two well-known methods, namely the interpolated cross-correlation function (ICCF; Gaskell & Sparke 1986; Gaskell & Peterson 1987) and the discrete correlation function (DCF; Edelson & Krolik 1988). In this work, cross-correlation analysis was performed between the V -band light curve and each of the NIR (J , H and K_s) light curves. Figure 3 shows the result of the cross-correlation analysis between V and J (upper panel), V and H (middle panel), V and K_s (lower panel). In each panel, the solid line shows the cross-correlation function (CCF) obtained by ICCF method, and the data points with error bars are those obtained by DCF method. Both ICCF and DCF are found to be in excellent agreement. The autocorrelation function (ACF) is also plotted for V -band (dashed-dot) and corresponding NIR band (dashed) in different panels. The ACFs show zero lag as expected, but the CCFs show an overall shift along the positive lag indicating that NIR continuum lags behind the optical V -band emission. The amount of lag can be estimated either by the lag corresponding to the peak of the CCF (τ_{peak}) or by the lag corresponding to the centroid of CCFs (τ_{cent}). The later has been found to be a better representative of the lag, particularly in cases when the light curves are either noisy and/or have less number of points (Peterson et al. 1998). The centroids of the CCF was calculated as

$$\tau_{\text{cent}} = \frac{\sum_i \tau_i \text{CCF}_i}{\sum_i \text{CCF}_i}. \quad (9)$$

To quantify the lag, we have used here the centroid of the CCF, which is evaluated by considering all the points that are within 60 per cent of the maximum of the CCF. This cut off was selected so as to have sufficient cross-correlation coefficients for the centroid determination.

The uncertainties in the derived lag were evaluated using a model-independent Monte Carlo simulation based on the flux randomization (FR) and random subset selection (RSS) described in Peterson et al. (1998) with the additional improvement as suggested by Wandel et al. (1999) and summarized by Peterson et al. (2004). In each Monte Carlo iteration, we first randomly took N independent points from a parent light curve of N data points regardless of whether any point has previously been selected. The new light curve after RSS method contains M data points. To take into account the uncertainty in the measured flux values, we then randomly modified the fluxes of the M data points by adding the uncertainties of the measured flux multiplied with a random Gaussian value. For each Monte Carlo iteration, we computed the CCF of the modified light curve and calculated the τ_{cent} using the points within 60 per cent of the CCF peak. This process was repeated for 20,000 iterations retaining only those CCF having peak value > 0.5 so that the cross correlation result is significant. We built the cross correlation centroid distribution (CCCD), which is shown by the histogram plot in each panel of Figure 3. The median of the CCCD is taken as a representation of the lag. Since the distribution has a non-Gaussian shape, we calculated uncertainties within 68 % confidence interval around the median value.

The result of the Monte Carlo simulation using different CCF analysis method is given in Table 3. The centroid lag obtained using DCF method was calculated for different bin sizes and the results are found to be consistent within error bars. The lags obtained by ICCF method are also given in Table 3 which agrees well with the DCF values within error bars. Though the time delays obtained from both DCF and ICCF agree with each other, for all further analysis we consider the lag obtained using the DCF with a bin size of $\Delta\tau = 5$ days as the typical sampling of our light curves is about 5 days. Based on this we find the rest frame (corrected for the redshift) time lags of $27.1^{+13.5}_{-12.0}$ days between V and J bands, $30.4^{+13.9}_{-12.0}$ days between V and H bands and $34.6^{+12.1}_{-9.6}$ days between V and K_s bands. Though there is an indication of wavelength dependent lag which increases with wavelength, because of the larger error bars, we conclude that within errors, the derived lags are consistent with each other. Considering only V and K_s light curves, we obtained a lag of $34.6^{+12.1}_{-9.6}$ days where K_s band variation lagging the V -band variations. This lag is larger than the lag of $3.01^{+0.42}_{-1.84}$ days obtained between the optical and emission line flux variations from optical spectroscopic monitoring observations (Stalin et al. 2011) and in agreement with what is expected from the unification model of AGN. Using this time delay we infer that the inner edge of the dusty torus is at a distance of $\approx 0.029^{+0.010}_{-0.008}$ pc from the central UV/optical AGN continuum source.

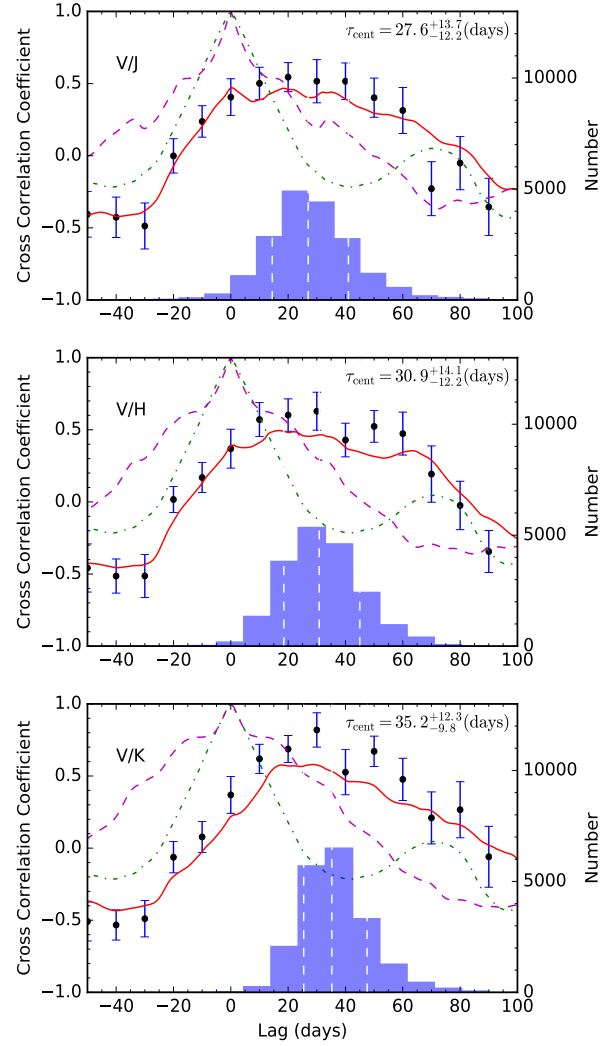


Figure 3. The CCF of V vs. J (top), V vs. H (middle) and V vs. K (bottom) is shown. In each panel, the solid line shows the ICCF, points with error bars show the DCF obtained using $\Delta\tau = 5$ days and the corresponding distribution of the τ_{cent} obtained using 20,000 Monte Carlo Simulations. The dashed-dot line shows the ACF of V -band light curve and the dashed line shows the ACF of corresponding NIR band light curve. The value of τ_{cent} obtained using Monte Carlo simulation is noted in each panel.

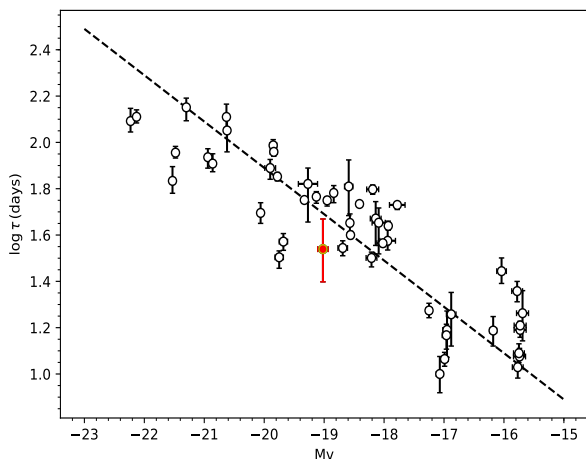
4 DISCUSSION

4.1 Infrared lag and central luminosity correlation

Using the rest frame time lag, the inner radius of the dusty torus in H0507+164 was found to be 0.029 pc. Similar measurements of the radius of the dust torus in about two dozen AGN are available in the literature based on DRM observations (see Koshida et al. 2014, and the references therein). These sources are shown in Figure 4 as empty circles in the lag - luminosity plane. Also, shown in the same Figure is the location of the source H0507+164 indicated by a filled circle. The best-fitted regression line $\log \Delta\tau = -2.11 - 0.2M_V$ of Koshida et al. (2014) which was based on a systematic and homogeneous analysis of DRM data of 17 Seyfert 1 galaxies is shown by a dashed line. Our lag measurement of

Table 3. Values of τ_{cent} and their associated errors in days as obtained by DCF (for various bin size ($\Delta\tau$)) and ICCF methods.

Bands	DCF ($\Delta\tau$ in days)					ICCF
	2	3	4	5	6	
$V - J$	$31.1^{+16.5}_{-15.0}$	$28.6^{+15.4}_{-13.8}$	$28.0^{+15.1}_{-12.2}$	$27.6^{+13.7}_{-12.2}$	$27.3^{+15.1}_{-12.0}$	$20.7^{+13.5}_{-11.0}$
$V - H$	$33.9^{+17.4}_{-14.8}$	$32.0^{+15.4}_{-13.6}$	$32.8^{+15.7}_{-14.0}$	$30.9^{+14.1}_{-12.2}$	$31.9^{+13.6}_{-12.6}$	$25.1^{+12.4}_{-11.0}$
$V - K_s$	$39.2^{+14.9}_{-12.3}$	$37.6^{+13.1}_{-11.1}$	$36.7^{+12.9}_{-10.7}$	$35.2^{+12.3}_{-9.8}$	$36.3^{+12.1}_{-10.7}$	$30.2^{+9.0}_{-7.9}$


Figure 4. Dust lag-luminosity relationship using the data of Koshida et al. (2014). The filled circle corresponds to the lag between the V and K_s bands determined for

H0507+164 which lies close to the regression line (dashed line), obtained by Koshida et al. (2014). The lag times were corrected for the time dilation effect using the object redshift.

H0507+164 is in excellent agreement with the lag expected for its luminosity and closely follows the dust lag-optical luminosity correlation of $\Delta\tau_{\text{dust}} \propto L^{0.5}$.

4.2 Structure of the BLR and the Dust Torus

Stalin et al. (2011) carried out spectroscopic reverberation observations of BLR of H0507+164 and estimated a lag between the optical/UV continuum and the $H\beta$ line emission of $3.01^{+0.42}_{-1.84}$ days in the rest frame of the object. Our DRM observations for the same object in different NIR wavelengths together with the result obtained by Stalin et al. (2011) provide important information about the structure of the BLR and the dust torus of H0507+164. The BLR lag is found to be smaller than the dust-lag (lag between V -band and K_s -band) which is as expected from the unified scheme of AGN. Though there are indications of a wavelength dependent lag in our multi-wavelength data reported here, they are not statistically significant due to the large errors in their lags. From an analysis of a sample of 17 Seyfert galaxies, Koshida et al. (2014) found that dust reverberation radius of their sample is 4-5 times larger than their BLR radius and typically a factor 2 smaller than their interferometric radius. Similarly, the BLR radius observed by reverberation

mapping is smaller than the same observed by NIR interferometry (see Petrov et al. 2012). Such difference is expected as the reverberation mapping is a response weighted radius originating from the compact region, while the interferometric radius is flux weighted sensitive to the flux coming from the outer region (Kishimoto et al. 2007). However, there are exceptions. For the source Mrk 335 (Du et al. 2014) NGC 4151 (Bentz et al. 2006) and NGC 4593 (Barth et al. 2013), the dust radius (Koshida et al. 2014) is about 10 times larger than the BLR radius. Such varied differences between the mean dust radius and BLR radius known in AGN will hint for variable dust emission (Koshida et al. 2009; Schnülle et al. 2015). To establish this, we need more precise measurements of dust radius for a large sample of AGN. Our ongoing multi-band DRM project on a larger sample will help to understand dust geometry.

5 CONCLUSION

We have presented the first measurements of the time delays between optical and NIR bands. This is based on optical V and NIR J , H and K_s bands observations spanning a time period of about 170 days. Significant variations have been observed in all bands. The rest frame lags between V -band and NIR bands are found to be $27.1^{+13.5}_{-12.0}$ days (V vs. J), $30.4^{+13.9}_{-12.0}$ days (V vs. H) and $34.6^{+12.1}_{-9.6}$ days (V vs. K_s). From the present analysis it is difficult to probe the existence of different lag between V and J , V and H and V and K_s , solely due to the large errors in the determined lags because of the limited amount of data analysed here. The presence of wavelength dependent lags if any can be established only with the accumulation of good quality monitoring data over a long period of time. It is likely that a combined analysis of the data would reduce the error in the lag between optical and NIR (Schnülle et al. 2015). Given the limited number of observations in the present work, we have not attempted a combined analysis.

Using the rest frame lag between V and K_s -band, we found that the inner radius of the dust torus is at a distance of 0.029 pc, from the central UV/optical continuum source. As expected from the unified model of AGN the dust inner radius is larger than the BLR radius known for this source from spectroscopic reverberation monitoring observations. Our estimate of R_{dust} and the V -band absolute magnitude is in good agreement with the dust lag-optical central luminosity relationship found by Koshida et al. (2014) from a large sample of AGN.

ACKNOWLEDGEMENTS

We thank the referee for his/her valuable comments that helped us to improve our manuscript. S.R. acknowledges the support by the Basic Science Research Program through the National Research Foundation of Korea government (2016R1A2B3011457). This research used the SIMBAD data base, which is operated at CDS, Strasbourg, France, the NASA/IPAC Extragalactic Database (NED), which is operated by the Jet Propulsion Laboratory, California Institute of Technology, under contract with NASA and data products from the Two Micron All Sky Survey, which is a joint project of the University of Massachusetts and the Infrared Processing and Analysis Center/California Institute of Technology, funded by the NASA and the National Science Foundation. We thank to the supporting staff at the Indian Astronomical Observatory (IAO), Hanle, and CREST, Hoskote. AKM and RS thank the National Academy of Sciences, India for providing the required fund for this project. SH acknowledges support from the European Research Council Horizon 2020 grant DUST-IN-THE-WIND (677117). P.G. thanks STFC for support (grant reference ST/J003697/2). MBP gratefully acknowledges the support from Department of Science and Technology (DST), New Delhi under the INSPIRE faculty Scheme (sanctioned No: DST/INSPIRE/04/2015/000108).

REFERENCES

Antonucci R., 1993, *ARA&A*, **31**, 473
 Barth A. J., et al., 2013, *ApJ*, **769**, 128
 Barvainis R., 1987, *ApJ*, **320**, 537
 Bentz M. C., Katz S., 2015, *PASP*, **127**, 67
 Bentz M. C., et al., 2006, *ApJ*, **651**, 775
 Blandford R. D., McKee C. F., 1982, *ApJ*, **255**, 419
 Burtscher L., et al., 2013, *A&A*, **558**, A149
 Czerny B., Elvis M., 1987, *ApJ*, **321**, 305
 Czerny B., Hryniewicz K., Maity I., Schwarzenberg-Czerny A., Życki P. T., Bilicki M., 2013, *A&A*, **556**, A97
 Du P., et al., 2014, *ApJ*, **782**, 45
 Edelson R. A., Krolik J. H., 1988, *ApJ*, **333**, 646
 Edelson R., Turner T. J., Pounds K., Vaughan S., Markowitz A., Marshall H., Dobbie P., Warwick R., 2002, *ApJ*, **568**, 610
 Enya K., Yoshii Y., Kobayashi Y., Minezaki T., Suganuma M., Tomita H., Peterson B. A., 2002, *ApJS*, **141**, 45
 Gaskell C. M., Peterson B. M., 1987, *ApJS*, **65**, 1
 Gaskell C. M., Sparke L. S., 1986, *ApJ*, **305**, 175
 Haas M., Chini R., Ramolla M., Pozo Nuñez F., Westhues C., Watermann R., Hoffmeister V., Murphy M., 2011, *A&A*, **535**, A73
 Hönig S. F., 2014, *ApJ*, **784**, L4
 Hönig S. F., et al., 2017, *MNRAS*, **464**, 1693
 Kishimoto M., Hönig S. F., Beckert T., Weigelt G., 2007, *A&A*, **476**, 713
 Kishimoto M., Antonucci R., Blaes O., Lawrence A., Boisson C., Albrecht M., Leipski C., 2008, *Nature*, **454**, 492
 Kishimoto M., Hönig S. F., Antonucci R., Barvainis R., Kotani T., Tristram K. R. W., Weigelt G., Levin K., 2011a, *A&A*, **527**, A121
 Kishimoto M., Hönig S. F., Antonucci R., Millour F., Tristram K. R. W., Weigelt G., 2011b, *A&A*, **536**, A78
 Kobayashi Y., Sato S., Yamashita T., Shiba H., Takami H., 1993, *ApJ*, **404**, 94
 Koshida S., et al., 2009, *ApJ*, **700**, L109
 Koshida S., et al., 2014, *ApJ*, **788**, 159

Lira P., Arévalo P., Uttley P., McHardy I., Breedt E., 2011, *MNRAS*, **415**, 1290
 Malkan M. A., Sargent W. L. W., 1982, *ApJ*, **254**, 22
 Meusinger H., Hinze A., de Hoon A., 2011, *A&A*, **525**, A37
 Minezaki T., Yoshii Y., Kobayashi Y., Enya K., Suganuma M., Tomita H., Aoki T., Peterson B. A., 2004, *ApJ*, **600**, L35
 Ninan J. P., et al., 2014, *Journal of Astronomical Instrumentation*, **3**, 1450006
 Oknyanskij V. L., Horne K., 2001, in Peterson B. M., Pogge R. W., Polidan R. S., eds, *Astronomical Society of the Pacific Conference Series Vol. 224, Probing the Physics of Active Galactic Nuclei*. p. 149
 Oknyanskij V. L., Lyuty V. M., Taranova O. G., Shenavrin V. I., 1999, *Astronomy Letters*, **25**, 483
 Peterson B. M., Wanders I., Horne K., Collier S., Alexander T., Kaspi S., Maoz D., 1998, *PASP*, **110**, 660
 Peterson B. M., et al., 2004, *ApJ*, **613**, 682
 Petrov R. G., Millour F., Lagarde S., Vannier M., Rakshit S., Marconi A., weigelt G., 2012, in *Optical and Infrared Interferometry III*. p. 84450W ([arXiv:1410.3108](https://arxiv.org/abs/1410.3108)), doi:10.1117/12.926595
 Pozo Nuñez F., et al., 2014, *A&A*, **561**, L8
 Rani P., Stalin C. S., Rakshit S., 2017, *MNRAS*, **466**, 3309
 Sánchez P., et al., 2017, *ApJ*, **849**, 110
 Sanders D. B., Phinney E. S., Neugebauer G., Soifer B. T., Matthews K., 1989, *ApJ*, **347**, 29
 Schnülle K., Pott J.-U., Rix H.-W., Peterson B. M., De Rosa G., Shappee B., 2015, *A&A*, **578**, A57
 Shields G. A., 1978, *Nature*, **272**, 706
 Stalin C. S., Jeyakumar S., Coziol R., Pawase R. S., Thakur S. S., 2011, *MNRAS*, **416**, 225
 Suganuma M., et al., 2006, *ApJ*, **639**, 46
 Tomita H., et al., 2006, *ApJ*, **652**, L13
 Vaughan S., Edelson R., Warwick R. S., Uttley P., 2003, *MNRAS*, **345**, 1271
 Wandel A., Peterson B. M., Malkan M. A., 1999, *ApJ*, **526**, 579
 Watson D., Denney K. D., Vestergaard M., Davis T. M., 2011, *ApJ*, **740**, L49
 Yoshii Y., Kobayashi Y., Minezaki T., Koshida S., Peterson B. A., 2014, *ApJ*, **784**, L11

This paper has been typeset from a $\text{\TeX}/\text{\LaTeX}$ file prepared by the author.